Reprint (R45)

An Introduction to Hyperspectral Imaging and Its Application for Security, Surveillance, and Target Acquisition

Reprinted with permission by P. Yuen and M. Richardson
Dept. of Informatics and Sensors, Cranfield University
The Image Science Journal

July 2010

Gooch & Housego

Gooch & Housego 4632 36th Street, Orlando, FL 32811
Tel: 1 407 422 3171 Fax: 1 407 648 5412 Email: sales@goochandhousego.com

An introduction to hyperspectral imaging and its application for security, surveillance and target acquisition

P Yuen* and **M Richardson**
Department of Informatics and Sensors, Cranfield University, Defence Academy of the United Kingdom, Shrivenham, Swindon SN6 8LA, UK

Abstract: This paper introduces the concept and principles of hyperspectral imaging (HSI) and it briefly outlines how the defence and homeland security sectors can benefit from the application of this extremely versatile technology. This paper outlines the pros and cons of the various HSI system configurations, with particular emphasis on two of the most commonly deployed spectrograph techniques, namely, the dispersive system and the narrow-band tuning filter system. It describes how HSI can be utilized for target acquisition particularly when there is no a priori knowledge of the target, and then shows how it can be used for the recognition and tracking of targets with desired or known signature characteristics. The paper also briefly mentions the possibility of remote HSI being used for recognizing a human's physiological state such as that induced by stress or anxiety. Real experimental data collected during the course of our research have been utilized throughout this paper to help understand the versatility and effectiveness of HSI technology.

Keywords: hyperspectral imaging, target detection, classification, automatic target recognition, remote sensing of intent, stress detection

1 INTRODUCTION

Hyperspectral imaging (HSI) is typically defined as a spectral sensing technique which takes hundreds of contiguous narrow waveband images in the visible and infrared regions of the electro-magnetic spectrum (Fig. 1).[1,2] The image pixels form spectral vectors which represent the spectral characteristic of the materials in the scene. Consequently, the technique has been applied mostly for material identifications and discriminations purposes. Although HSI was originally developed for mining and geology applications, its usage has quickly spread into other civilian sectors and more recently into the military sector due to the ability to discriminate between materials.[3] In military and security applications, the technique has been specifically adopted for the detection and recognition of targets which are normally well camouflaged with respect to the background and hence, HSI is designed as a counter-countermeasure allowing 'look-alike' targets to be acquired[4] and this is illustrated in Fig. 2, which depicts the red/green/blue (RGB) image of an apparent green leafy plant (Fig. 2a), where in fact there is only one live leaf and the rest of the leaves are artificial. Modern decoys and camouflage materials can be made with high degrees of sophistication to mimic the background characteristics as shown in Fig. 2c, in which the spectral characteristics of the camouflaged target exhibits a mere 2% difference with respected to that of the background. However, Fig. 2c shows subtle spectral differences of the target with respected to the background and these mostly occur in small

The MS was accepted for publication on.
* *Corresponding author: Peter Yuen, Department of Informatics and Sensors, Cranfield University, Defence Academy of the United Kingdom, Shrivenham, Swindon SN6 8LA, UK; email: p.yuen@cranfield.ac.uk*

ONLINE COLOUR ONLY

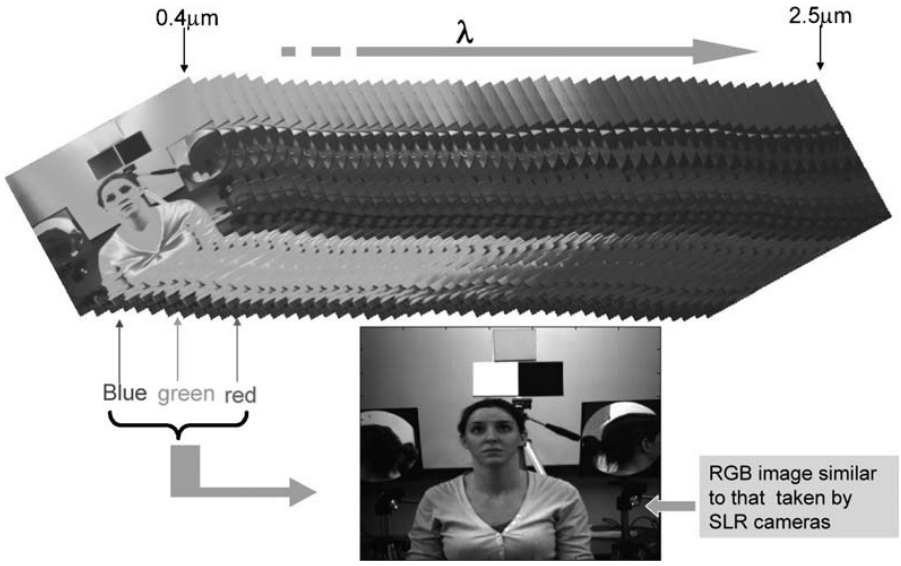

1 Introduction of the concept of hyperspectral imaging (HSI) which is literally a technique that takes many contiguous narrow-waveband images instead of just the three broad bands of red, green and blue colours in the conventional digital photography process

bandwidths nominally of the order of ~10 nm. An integration of the two traces over a broad spectral range would give almost two identical outputs. This highlights the need of a technique like HSI which exploits information at a high spectral resolution over a wide spectral range to allow the subtle spectral contrast to be detected. One purpose of this paper is to introduce the versatility and effectiveness of this technique for target detection and recognition and how this has made HIS one of the most powerful remote sensing counter-countermeasures techniques to date.

This paper briefly describes the main features of the HSI technique and outlines how it can be utilized for defence and homeland security applications, and examples are given in the context of real data extracted from the work being conducted within the Sensors Group of the Defence Academy, Cranfield University.

2 FUNDAMENTALS OF HSI

2.1 HSI instrumentations: an overview

HSI uses large numbers of contiguous narrow bands of wavelength information to create spectral vectors in each pixel of the scene, forming a hyperspectral cube (again see Fig. 1) which contains two spatial dimensions together with one spectral dimension.[1,2] In the heart of the HSI instrumentation is the spectral dispersion mechanism which is known as spectrograph, and it exists in various different forms of which the most common three categories have been the dispersive spectrometer, the Fourier transform interferometer and the narrow-band tuneable filter. Details of these spectrographs can be found in the literature by Vagni,[5] and the principles of the most commonly employed dispersive and tuneable filter spectrographs for HSI instrumentation are briefly outlined here.

2.2 Dispersive spectrograph

A dispersive imaging spectrometer uses either a grating or a prism for light dispersion, and the hyperspectral cube is formed by coupling the dispersing element with a two-dimensional array of detectors such that the spectral 'image' is formed along one axis of the sensor. This produces one line of the scene image and hence to generate a full hyperspectral image cube, a scan technique/mechanism is required along the other axis. A prism-based system has advantages of having high efficiency and low scatter, but their optical design tends to be considerably more complex than their grating-based counterparts.

Gratings can be optimized to achieve high optical power for a certain order of interference within a specific wavelength region. The spectral resolution of a grating is proportional to the order and to the number of lines in the grating, and it is constant over

The Imaging Science Journal imsIR6.3d 13/7/10 09:02:54
The Charlesworth Group, Wakefield +44(0)1924 369598 - Rev 7.51n/W (Jan 20 2003)

ONLINE COLOUR ONLY

a b (c)

2 The common usage of HSI for material discrimination: (a) RGB image: the RGB picture of a green plant; (b) NIR composite image: the image of the same plant and using a composite of three selected wavelengths in the visible and near-infrared region, it successfully discriminates the live leaf (in green) from the fake (in blue and red); (c) spectral characteristics of camouflage target: it emphasizes why HSI is useful for counter-countermeasures: the spectra of a camouflaged target are shown compared with the surrounding background and subtle spectral differences over very small bandwidths are discernable but broad-band imaging would not be able to tell these two spectra apart

the image plane for a constant incident angle of the radiation. In a grating spectrometer, the prism is replaced by either a transmissive or reflective grating and in the all-reflective optical design, the grating system can achieve high efficiencies of about 85%. There are two forms of gratings and the most common one has been the convex grating utilizing the Offner spectrometer design as that illustrated in Fig. 3. The gratings of this type tend to be small, typically $\sim$25 mm diameter. The advantages of the Offner spectrometer are that it operates with a relatively low F number (about $F/2$) and it is a reasonably simple and compact design. Figure 3a shows the Offner convex spectrograph schematic, Fig. 3b shows the integration of the spectrograph with its objective lens and Fig. 3c shows the completed visible and near-infrared (VNIR) HIS camera with the mirror scanning assembly on the top.

The other design of the dispersive imaging spectrograph uses both the dispersing elements of a prism and a grating in a single package. This is generally achieved using a specially designed volume transmission grating which is cemented between two almost identical prisms. This design is commonly known as prism–grating–prism (PGP)[7] as shown in Fig. 4a. The PGP has the advantage of preserving the optical axis but with a penalty of losing transmittance due to the fact that materials with high dispersion also

ONLINE COLOUR ONLY

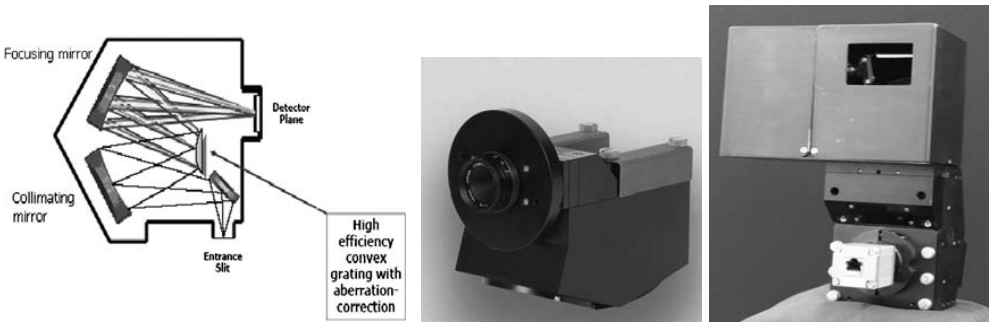

(a) b c

3 (a) The schematic ray diagram of the Offner convex spectrograph; (b) the compact housing for the Offner spectrograph manufactured by the Headwall Photonics;[6] (c) the complete visible and near-infrared (VNIR) HSI camera in the Sensors Group, consisting of the Headwall's spectrograph and a two-dimensional array camera system and the Sensors Group-designed and -built mirror scanner assembly (situated at the top of the spectrograph)

The Imaging Science Journal imsIR6.3d 13/7/10 09:02:55
The Charlesworth Group, Wakefield +44(0)1924 369598 - Rev 7.51n/W (Jan 20 2003)

ONLINE COLOUR ONLY

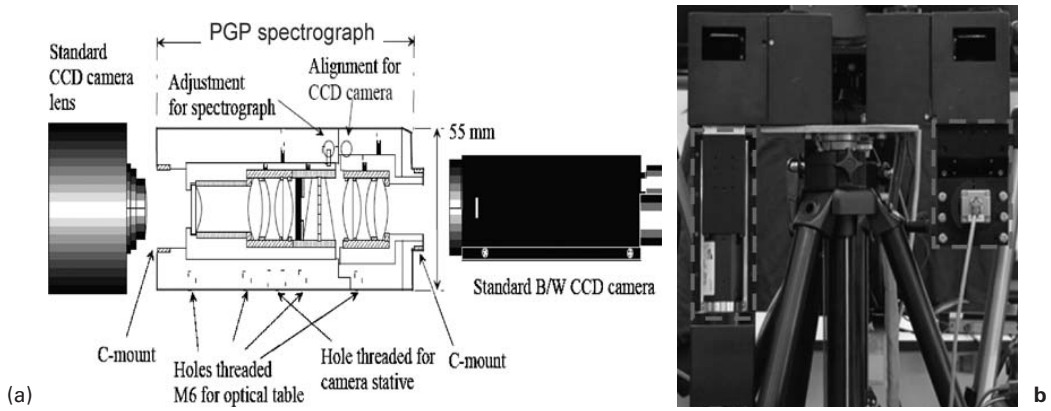

4 (a) The design of a PGP-based spectrograph;[7] (b) the two line scanning hyperspectral cameras in the Sensors Group. On the left is the PGP-based camera and on the right is the Offner VNIR system. The dashed rectangles depict the physical dimensions of the two spectrographs showing the compactness is the Offner design in comparison with the PGP design

usually exhibit high absorption which results in a reduction of the overall throughput of the system. Owing to the linear layout of the PGP, the physical dimension of the PGP spectrometer is more extensive than that of the Offner design and this can clearly be seen in Fig. 4b with the PGP spectrometer system on the left in comparison to the Offner system on the right.

2.3 Narrow-band tuneable filters

One of the drawbacks of using a dispersive spectrograph in HSI instrumentation has been the limitation of the system to operate in a line scanning mode and the requirement either to move the imaging system or the need of some other form of scanning devices in order to capture the full hyperspectral cube of the scene. One of the technologies developed to remedy this has been the use of narrow band tuneable filters. These have the characteristic ability to transmit electromagnetic radiation through a very narrow bandpass of spectral region (bin) over a wide spectral range. Filters like circular or linear variable filters, acousto-optical tuneable filters (AOTF) and liquid crystal tuneable filters (LCTF),[5,8,9] have been implemented in step stare mode operations such that snap shots of the whole scene at the bandpass wavelengths can be taken in a sequential manner. Among these filters, the AOTF and the LCTF have been the most popular[10] for multispectral imaging (MSI) implementation.

The AOTF makes use of light diffraction within a piezoelectric crystal such as TeO_2, by passing an acoustic wave simultaneously with the light beam through the crystal. There are several different configurations and the acoustic wave can be propagated orthogonally or in parallel to the input light beam. When an acoustic wave is propagated through the piezoelectric crystal, the refraction index of the crystal is modulated by the alternating planes of compression and rarefaction of the travelling ultrasonic wave. This is shown schematically in Fig. 5a where the crystal behaves like a grating which diffracts light of a specific wavelength into a beam stop or a polarizer, and the diffracted beam is then sensed by the sensor. At a given wavelength of the acoustic wave λ_a, the diffracted light at the passband of λ_l can be given by

$$\lambda_l = \delta_n \alpha \lambda_a \tag{1}$$

where δ_n is the birefringence of the crystal and α is a parameter dependent on the design of the AOTF system. The diffraction efficiency of an AOTF is proportional to the strength of the acoustic beam and it can achieve a maximum of $\sim 90\%$ split between the two polarized diffracted beams with a net throughput of about 30–45% in each beam. The spectral range of the AOTF depends very much on the characteristics of the crystal as well as on the size of the angular aperture, which tends to reduce the overall useable spectral range when a large angular aperture is used. In practice, the crystal utilizes small aperture sizes of about 12×12 mm with a field of view (FOV) of $\sim 4^\circ$ and is capable of producing a spectral range of about 500–850 nm.[10,11] In general, the crystal is driven using a very small range of acoustic frequencies δf_a centred at f and this effectively broadens up the transmission characteristic by $\lambda_l \pm \delta\lambda_l$ allowing a user selected bandpass width (Fig. 5b). As shown in

The Imaging Science Journal imsIR6.3d 13/7/10 09:02:57
The Charlesworth Group, Wakefield +44(0)1924 369598 - Rev 7.51n/W (Jan 20 2003)

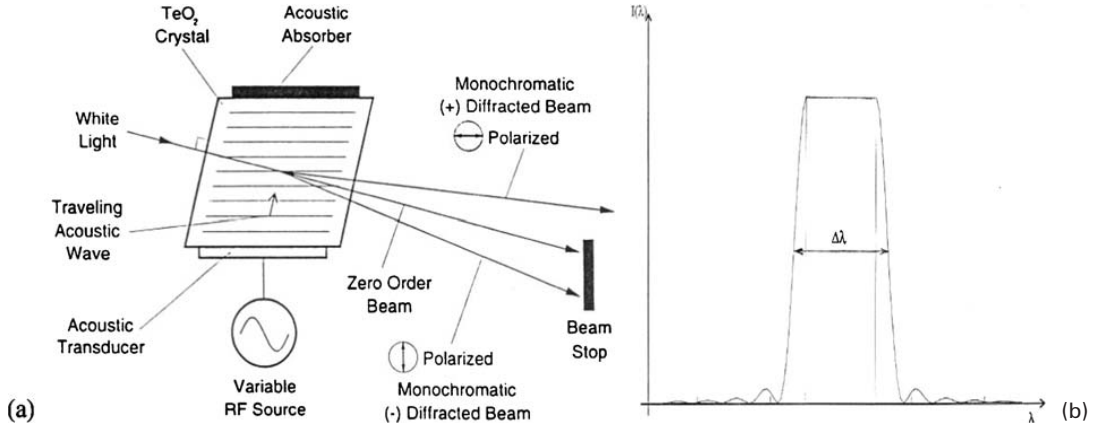

5 In (a) it shows the schematic working principle of AOTF for MSI illustrated using the TeO_2 as the piezoelectric crystal and operated in a non-collinear configuration.[8] One important characteristics of the AOTF MSI is the flexibility of tuning, which not only allows the user to select the pass wavelengths in any spectral order, but also enables a variable band width of the passband as shown in (b)

equation (1), the diffracted beam λ_1 can be changed by alternating the frequency of the acoustic wave, thus giving a complete electronically tuneable optical filter without any moving parts. Furthermore, the λ_1 can be tuned either sequentially or even randomly in any spectral order; something that the grating-/prism-based spectrometer could never attain. The tuning times are typically in the order of microseconds and consequently, the AOTF system remains as one of the most suitable candidates for applications which require high-speed MSI, such as those in surveillance requiring real-time video recordings. Figure 6 shows the AOTF system used in the Sensors Group, comprising a VNIR AOTF together with a third-party CCD camera (Andor Ixon 897) and the system is capable of delivering $\sim$50 frames per second at 512×512 pixel resolution. The spectrograph is made by Gooch & Housego Photonics[10,11] and this system is being used for homeland security research.

3 HSI FOR TARGET DETECTION APPLICATIONS

3.1 Target detection without prior knowledge: anomaly detection

On many occasions, particularly in strategic deployments during conflicts in the battlespace, the exact form of an opponent's targets being deployed in the field is not always known. These targets, especially when they are deployed in uninhabited scenarios such as dessert, mountain or forest terrains, where the background is distinct from man-made objects like military vehicles or mines, can be readily detected as anomalies using HSI techniques even though they may have been camouflaged.

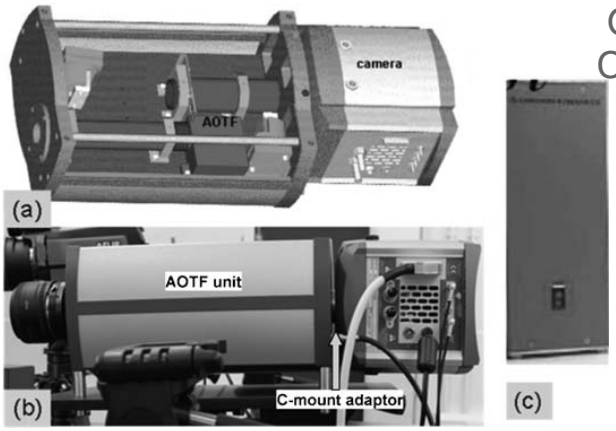

ONLINE COLOUR ONLY

6 (a) shows the graphical representation of the AOTF system in the Sensors Group for imaging in the 500–900 nm spectral range using TeO_2 as the active crystal: the figure shows the associated steering optics together with the AOTF spectrograph which is made by Gooch & Housego Photonics[10,11] with transmission characteristics of $\sim$35%, and a high-end CCD camera (Andor Ixon 897). Owing to the small FOV ($\sim 4^\circ$), a 50 mm objective lens is deployed as shown in (b). The AOTF is coupled with the camera via a standard c-mount adaptor which makes the AOTF a very versatile add-on component, and the unit is powered via a separate driver box through standard BNC interface (c)

The Imaging Science Journal imsIR6.3d 13/7/10 09:02:58
The Charlesworth Group, Wakefield +44(0)1924 369598 - Rev 7.51n/W (Jan 20 2003)

ONLINE COLOUR ONLY

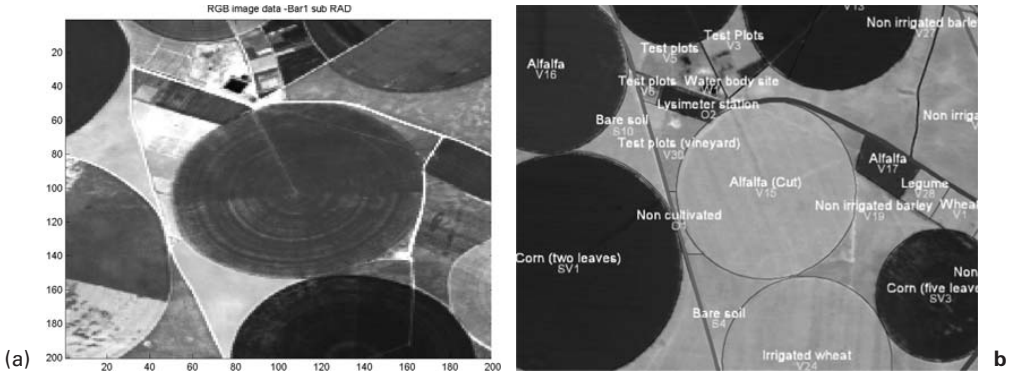

7 The Barrax HSI dataset which consists of various crops and vegetation: (a) the RGB image of the scene; (b) the area use map of the scene and adjacent area. Note that this imagery contains at least three distinct kinds of materials: green and brown crops and bare soil. There is a water body/tank and some other man-made agricultural equipments behaving as anomalies in the natural environment

There is a great variety of detection algorithms proposed for HSI remote sensing applications and among these, the anomaly detection (AD) technique[12,13] that identifies pixels with spectral characteristics different from that of the background without priori information, has received considerable attraction within the community. There are quite a few AD algorithms reported in the field, but most of them are based on the one derived by Reed and Yu, which is widely known as the RXD[14]

$$\phi_{\mathrm{RXD}} = (x-\mu)^{\mathrm{T}} \Gamma^{-1}_{\mathrm{background}} (x-\mu) \qquad (2)$$

where x is the HSI data in a matrix of pixel x band, μ is mean of the background pixels, $\Gamma_{\mathrm{background}}$ is the band to band spectral covariance of the background which has been modelled as a multivariate Gaussian like density, and T is the matrix transpose. There exist many other forms of AD such as the low probability detector, the uniform target detector,[15] the spectral descriptive signature anomaly detector,[16] the kernel RX,[17,18] etc., all of which are based on the RXD framework but vary in the way the background is characterized or how the data are projected into the appropriate subspace. Recent research in this area has been the improvement of RXD for subpixel target detection[19] as well as enhancing detection performances using a multiple algorithm fusion approach.[4]

3.1.1 Anomaly detection in a vegetation background

To illustrate the effectiveness of anomaly detection using HSI technique, the hyperspectral dataset of an agricultural site which was recorded in Barrax, Spain, during the ESA Digital Airborne Imaging Spectrometer Experiment campaign in 1999, is employed here as an example. The flight altitude was 4 km and every image pixels in the scene represents 3 m on the ground. The dataset contains various types of green vegetation, brown crops and bare soil as shown in the RGB image of the scene presented in Fig. 7a. The land use map of this scene is depicted in Fig. 7b and has indicated the presence of a metallic water tank together with some agricultural equipments which are the only man-made materials within this agricultural site.

Using an algorithm known as MUF2 which is based on the principle of equation (2) but utilizes a multiple approach fusion methodology,[4] the result as shown in Fig. 8 has achieved 100% detection of anomalies while keeping the false alarm rate at 0.0002 for this Barrax dataset. This means that there are two false alarms for every 10 000 image pixels in this detection. To aid visual convenience, the detection result has been overlaid on top of the RGB presentation of the scene and the combined image is depicted in Fig. 8, showing the correctly identified anomalies in red, while the false alarms have been presented in yellow. This shows the extremely high detection rate achieved using this HSI technique even when knowledge of the target signature is absent.

3.1.2 Anomaly detection in a desert environment: surface mine detection

The detection of small targets such as surface laid mines is known to be difficult, particularly at long standoff ranges. It is therefore of great interest to

The Imaging Science Journal imsIR6.3d 13/7/10 09:02:59
The Charlesworth Group, Wakefield +44(0)1924 369598 - Rev 7.51n/W (Jan 20 2003)

ONLINE COLOUR ONLY

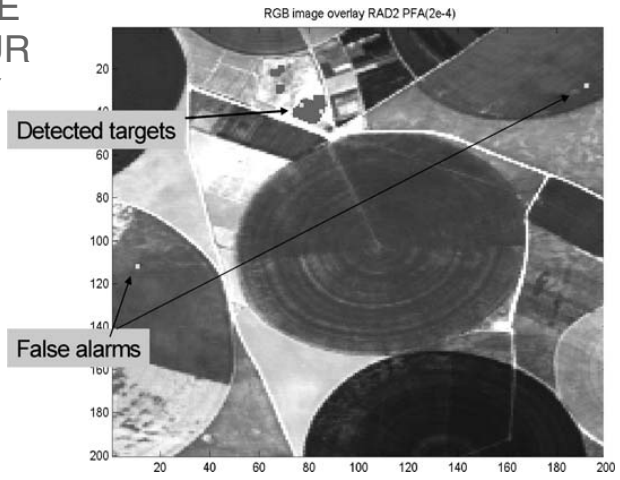

8 The detection result at a false alarm rate of 0.0002 using the MUF2 anomaly detection algorithm,[4] and the result is overlaid onto the RGB image of the Barrax scene to help visualisation of the effect. The detection is presented by red pixels for the correctly identified targets, and in yellow to represent the false alarms. The probability of detection is 100% with only 8 false alarm pixels in total over the complete scene, showing the extreme efficiency for the detection of anomalies using HSI technique

assess the effectiveness of HSI techniques for the detection of these small cross-section targets within backgrounds of an inhomogeneous nature like those shown in Figs. 9 and 10. The dataset was taken in May 2005 in the Anza Borrego desert, San Diego, CA, USA, and the arid region scene containing various plants and bushes as clutter background. A set of plastic plates of $\sim$0.3 m diameter are used to represent the surface-laid mines and are placed in rows onto the surface of a road/track junction. Three rows are laid directly onto the surface and one row is buried under a thin layer of sand. Some of the plates have been camouflaged in sand-like colours, and the dataset was recorded at a range of $\sim$0.5 km with an effective ground sampling distance (GSD) of $\sim$0.3 m resulting in comparable pixel and target dimensions. The dataset exhibits some strip noise due to sensor motion on the host aircraft.

Figure 11 shows the anomaly detection result using the MUF2 algorithm[4] and as in the previous section, the detection result is overlaid onto the RGB presentation of the dataset with red pixels depicting the correctly identified targets (man-made objects), and the false alarms are marked in yellow. The result presents a detection accuracy of $\sim$0.6 at the false alarm rate of 0.003, which is almost an order of magnitude worse than that of the Barrax result. The main cause of this relatively low performance has been due to the very small detection cross-sections of the targets and the very noisy nature of this dataset. These issues are important to military deployments and they are being addressed in our current research using an adaptive band selection approach.

3.2 Detection with prior knowledge: material discrimination and matched filter detection

It is quite common that the materials to be identified in a given scene have known signature characteristics, and thus, the task has become how to find these characteristics from the clutter of the background. In conventional machine vision tasks, the textural patterns are used for target recognitions, whereas the spectral characteristics have been the primary information employed by HSI for material discriminations. In our work, we have taken the step of using textural,

ONLINE COLOUR ONLY

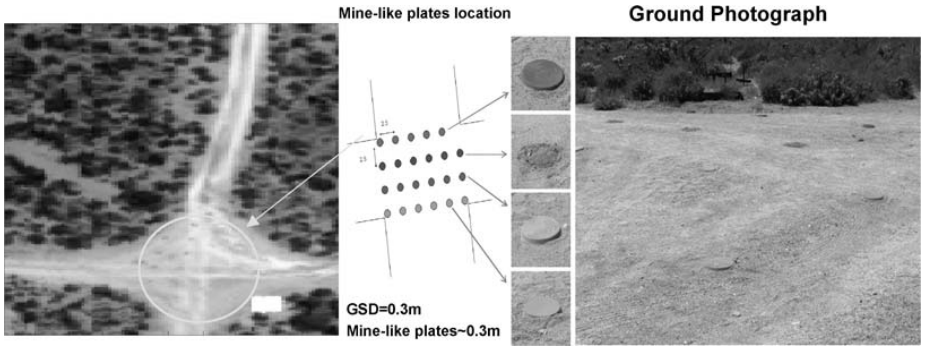

9 The desert trial data of the Anza Borrego desert imaged at a range of $\sim$0.5 km with an effective GSD of 0.3 m. The targets are plastic plates of diameters $\sim$0.3 m with green and sand-like colours; they are laid in rows on the surface but with one row buried in the sand as shown in the ground photographs in the right hand panel. A set of five calibration panels is located just next to the target field for assisting radiometric calibration

The Imaging Science Journal imsIR6.3d 13/7/10 09:03:00
The Charlesworth Group, Wakefield +44(0)1924 369598 - Rev 7.51n/W (Jan 20 2003)

ONLINE COLOUR ONLY

10 The ground photographs of the clutter background in the desert trial data consisting of various species of cacti, small bushes, medium sized trees, a road track and sand. This scene is considerably different from the Barrax data (Fig. 7) having a larger material variation with many different species randomly scattered throughout the scene

spectral and temporal information within the framework of a statistical and a cortex-like neuromorphic approach for automatic target recognitions.[20] This section introduces the technique of a matched filter detection algorithm for the identification of materials with known signature characteristics.

In the language of machine, learning the process for the identification of objects with given priori knowledge is known as supervised classification. With no priori knowledge, the process is known as unsupervised classification. Target detection is a subset of classification in which the detection process attempts to classify pixels into two classes of target or background, while classification in general attempts to cluster pixels into different classes according to the statistics of some measured metrics. The advantages of supervised classification are that it is simple to implement and its performance is relatively superior to unsupervised classification. Examples of popular supervised classification schemes for the hyperspectral remote sensing application have been spectral angle mapping, maximum likelihood, neural net, support vector machine, linear discriminant classifier (matched filter) and other distance metrics such as Mahalanobis and minimum distance.[12,21]

ONLINE COLOUR ONLY

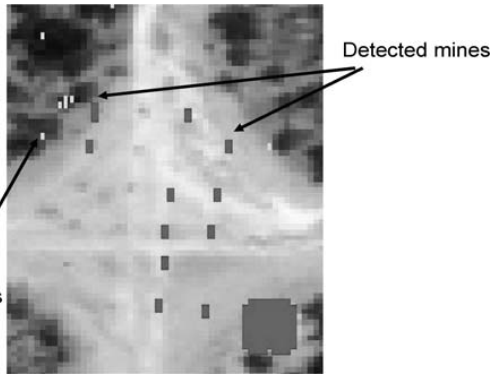

11 shows the detection result at a false alarm rate of 0.003 using the MUF2 anomaly detection algorithm,[4] and as before, the result is overlaid onto the RGB image of the scene to help visualisation of the result. Again, the correctly identified targets (man-made objects) are in red and the false alarms are in yellow. The probability of detection achieved at this false alarm rate is ~ 0.6, which is almost an order of magnitude lower than that of the Barrax dataset. This is mainly caused by the very small detection cross-section of the mines and the noisiness of the dataset

Almost all parametric supervised classifiers extract class parameters, such as the class covariance Γ and the class mean μ, exclusively from the training data. In the classifier such as the quadratic classifier, the goal is to evaluate the likelihood function H for each class and the pixel x will be assigned to class label k if $H_k(x) > H_i(x)$ for all $i \neq k$ class labels, and this is commonly termed as the maximum likelihood classifier. In this case, the likelihood function is in the form of[21]

$$H_i(x) = |\Gamma_i| + (x_i - \mu_i)^T \Gamma_i^{-1} (x_i - \mu_i) \tag{3}$$

where the parameters γ_i and μ_i are the in-class covariance and in-class mean, respectively. In situations such as surveillance applications, the number of target pixels is normally a small fraction of the total number of image pixels in the scene and the sparseness of the target class implies that there are not sufficient data to train a statistical classifier for target classifications. This is a well-known issue with small sample size problems and there are various ways that can be employed for improving the classification parameterisation.[22] Alternatively, a slightly different formulation using Fisher's linear discriminant known as the spectral matched filter can be used[12]

$$y(x_i) = \frac{\mathbf{s}^E \Gamma_b^{-1} x_i}{\mathbf{s}^T \Gamma_b^{-1} \mathbf{s}} \tag{4}$$

The Imaging Science Journal imsIR6.3d 13/7/10 09:03:04
The Charlesworth Group, Wakefield +44(0)1924 369598 - Rev 7.51n/W (Jan 20 2003)

ONLINE COLOUR ONLY

a b

12 (a) shows the photograph of a car park scene and there are some t-shirts scattering around the site acting as targets. The signatures of seven selected t-shirt as targets have been pre-assessed in the laboratory under artificial illumination condition as shown in (b)

where **s** is the spectral signature of the target which can be extracted either from a library or through the mean of the training dataset, and Γ_b is the out-of-class covariance which is quite different from the covariance γ_i in equation (3). If the value of $y(x_i)$ is larger than a preset threshold and then the pixel at i will be assigned to the same class label as the target **s**.

Shown in Figs. 12–14 is an example of how the desired targets can be detected from the field using the basic matched filter detection according to equation (4). Figure 12*a* depicts the RGB image of a car park scene, and the desired targets are the coloured t-shirts representing pedestrians and they are placed among the gaps between the cars. The spectral signatures of these targets have been pre-assessed in the laboratory under artificial lighting illumination, as shown in Fig. 12*b*. It is quite obvious that the recorded raw data sensed by the HSI instrument are illumination-dependent, and the at-sensor signal has been compounded by the sensor's characteristic as well as the camera settings. This is illustrated in Fig. 13a showing the two spectra of a light green t-shirt which have been recorded in the laboratory and outside in the field, and two different spectra for the same target are shown. Thus, it is essential to extract the intrinsic characteristics such as the reflectance of the target to achieve an environment invariance property and to use this as the target signature characteristic. This is commonly attained through a process known as atmospheric correction which recalibrates the scene into its intrinsic characteristic[23,24] such that its property will be invariant in time, space, surface properties of the material concerned, illumination conditions and spatial varia-

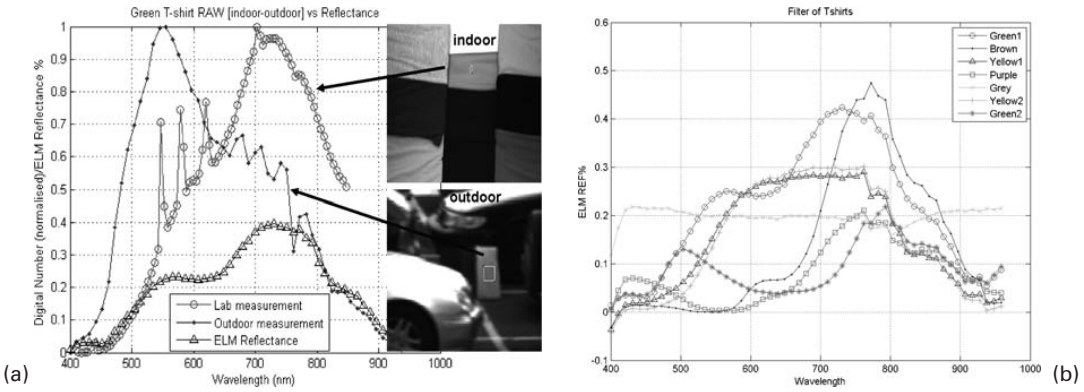

(a) (b)

ONLINE COLOUR ONLY

13 The real need to convert the raw HSI data into its intrinsic reflectance before the detection: (a) two distinctly different spectra of the same material (green t-shirt) recorded under two different environments of indoor and outdoor illuminations, which are in turn very different from its intrinsic reflectance as depicted in the black triangle plot; (b) the reflectance spectra of all the t-shirt targets which were measured in the laboratory and they were then converted into reflectance using an atmospheric correction scene calibration method

The Imaging Science Journal imsIR6.3d 13/7/10 09:03:06
The Charlesworth Group, Wakefield +44(0)1924 369598 - Rev 7.51n/W (Jan 20 2003)

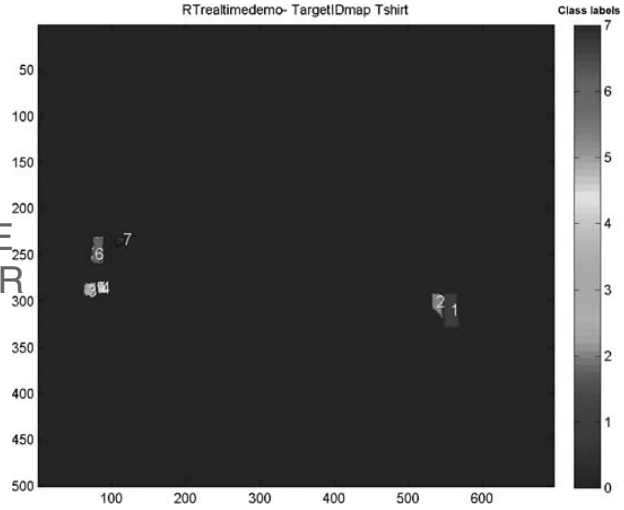

14 The detection result obtained by the basic matched filter algorithm, aiming at the detection of the seven selected t-shirts that have been presented in Fig. 12b. All pixels are in false colours according to the colours of the class labels located on the right hand side of the figure. Class 0 represents the background and anything else that does not belong to any of these seven targets

tions on the ground. Figure 13b shows the reflectance traces of the seven selected t-shirt targets which were measured in the laboratory, and they were then used as the target signatures for finding the t-shirts in the car park scene that is presented in Fig. 12a.

Using the reflectance spectra of the t-shirts presented in Fig. 13b as the target vector **s**, the matched filter detection result in false colours is shown in Fig. 14. The result highlights the detected target pixels in different colours according to the colour of the class labels as depicted in the right hand colour bar of the figure. There are seven class labels representing the seven different colours of the t-shirts as shown in Fig. 12b, and in addition, there is a class 0 which represents the background to include everything else that does not belong to any of these seven classes. It is quite clear that the result has got a majority of class 0 pixels and only six out of the seven targets have been found. The detection performance has been good but not completely ideal; hence, current research in our laboratory has been using more sophisticated classifiers together with adaptive feature selection methodology for the recognition and tracking of pedestrians and vehicles in a highly cluttered background such as that in the town centre.

3.3 Remote sensing of stress for homeland security applications using HSI

Technologies for the combat of terrorism have been one of the fastest growing demands in the twenty-first century's homeland security sector. There have been numerous novel ideas proposed for anti-terrorism,

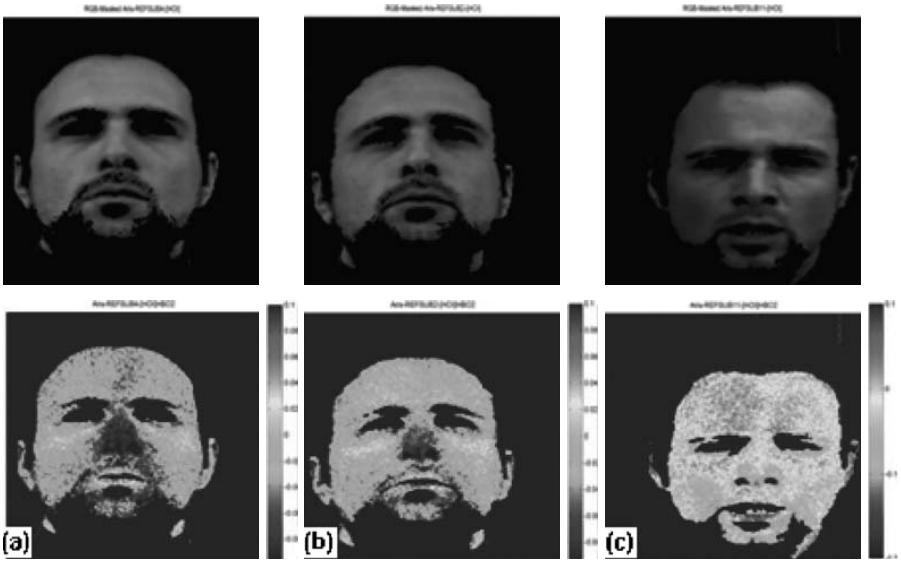

15 The result for the detection of emotional and physical stress by sensing the increases in blood oxygenation using an HSI technique. The upper and lower panels are the RGB pictures and the oxy-haemoglobin (HbO_2) maps in false colours respectively when the subject was at rest (a), under emotional stress (b) and under physical stress (c). The HbO_2 level is represented by the hotness of colour: bright red=100% and dark blue=0%. It is seen that the HbO_2 level increases when the subject is under emotional and physical stress

The Imaging Science Journal imsIR6.3d 13/7/10 09:03:07
The Charlesworth Group, Wakefield +44(0)1924 369598 - Rev 7.51n/W (Jan 20 2003)

and one of the most important ones has been the direct detection of improvised explosive devices (IED). Relatively indirect methods such as through human behaviour, activity, contextual and body language (gestures and facial expressions) have been proposed for the extrapolation of motive via a human factors computational model. When explosives are packed in a light and air tight manner, it is clearly a technical challenge to detect them directly. Indirect methods using an 'effective computing' approach relies a great deal on the certainty of cognitive theories which is itself a matter of intensive research. Other direct methods, such as to assess intent through physiological or neurological states, are viable but challenging in practice. Conventional means for assessing intent have been by direct contact methods such as polygraph and functional magnetic resonance imaging, and both these techniques are not feasible for implementation in busy public places.

So rather than detecting the IED directly, we are seeking to discern if intent can be assessed through physiological or neurological states, such as the detection of human stress. Stress is a temporarily-induced physiological and/or psychological imbalance that is caused by any action/situation (stressor) which an individual regards as a possible danger or threat. A physical stressor is one that has a direct effect on the body. This may be an external environmental condition (heat, cold and noise) or due to the internal physical/physiological demands of the human body such as caused by physical exercise. A mental (emotional) stressor is one in which only information reaches the brain with no direct physical impact on the body. This information may place demands on either the cognitive systems (thought processes) or the emotional system (feeling responses, such as anger or fear) in the brain.

It is well-known that emotional or physical stresses induce a surge of adrenaline in the blood stream under the command of the sympathetic nervous system, which cannot be easily suppressed by training. The onset of this alleviated level of adrenaline triggers a number of physiological chain reactions in the body, such as dilation of the pupil and an increased level of blood flow to muscles. There is evidence that the result of these physiological responses causes an elevation of blood oxygenation in the body by approximately two-fold during stress, and thus it is possible to detect these changes of oxygenation as an indication of stress level using imaging techniques such as HSI.[25]

Spectroscopic tuning has been a common method for assessing tissue haemoglobin oxygenation,[26,27] and generally, it is realized using a selection of a few wavelengths which exhibit strong differential absorptivity characteristics. Using the Beer Lambert law formulation, each constituent in the region of interest can be deduced through the relationship

$$\mathbf{A} = \sum \alpha_i C_i \tag{5}$$

where **A** is the attenuation of the probing light, and α and C are the wavelength-dependent absorption coefficient and concentration of each constituent *i* in the tissue sample. Most workers in the field assumed that the haemoglobin and the melanin are the only main scatters in the visible region <600 nm. Owing to the appreciable penetration of light into the body tissue for wavelengths in the near-infrared region between 600 and 1000 nm, it is found that as many as six different wavelengths in this region are needed in order to solve equation (5) for deducing the concentrations of various substances contained within the probing depth. Using three different wavelengths at around the 550 nm region, we have developed two different algorithms to successfully detect the stress via haemoglobin oxygenation analysis. Figure 15 shows the level of oxy-haemoglobin (HbO_2) of a participant in false colours when he was under emotional and physical stress. The hotness of the colour represents the levels of the HbO_2 with bright red pixels being 100% and a dark blue being 0%. It is seen that the HbO_2 increases particularly in the facial region when the subject is under both emotional and physical stress. This result was obtained during a preliminary study carried out in 2009 and that the detection algorithm utilized had not been optimized and continued improvements are a matter of ongoing research in our laboratory.

4 CONCLUSIONS

This paper introduces the concept of HSI and highlights the pros and cons of various instrumentation options of the technology particularly for military and homeland security applications. The paper has covered two of the most commonly deployed spectrograph types in the HSI community, namely, the dispersive and the narrow-band tuning filter. It then follows on to highlight how HSI can be adopted for target detections particularly when the knowledge of the target is not available, and also how

The Imaging Science Journal imsIR6.3d 13/7/10 09:03:09
The Charlesworth Group, Wakefield +44(0)1924 369598 - Rev 7.51n/W (Jan 20 2003)

it can be used for the recognition and tracking of objects with desired signatures. The paper has also briefly demonstrated the possibility for recognizing human physiological states such as those induced by stress or anxiety using HSI at a standoff distance. By monitoring the haemoglobin oxygenation level in the facial region, we have shown a successful detection of stress through an increase in oxy-haemoglobin level. Throughout this paper, the versatility of HSI for defence and homeland security applications has been emphasized using real experimental data collected during the course of our research with the Sensors Group here at the Defence Academy.

ACKNOWLEDGEMENTS

The authors would like to thank the UK MOD and the UK EPSRC for the support of our work in the areas of machine vision and HSI research.

REFERENCES

1 Shaw, G. and Burke, H. Spectral imaging for remote sensing. Lincoln Laboratory J., 2003, **14**, 3–28.
2 Smith, R. 'Introduction to hyperspectral imaging', http://www.microimages.com/getstart/pdf/hyprspec.pdf
3 Goldberg, A. C., Stann, B. and Gupta, N. Multispectral, hyperspectral, and three-dimensional imaging research at the U.S. Army Research Laboratory, Proc. Sixth International Conference of Information Fusion: Fusion 2003, Cairns, Qld, Australia, July 2003, International Society for Information Fusion, pp. 499–506.
4 Yuen, P. and Bishop, G. Hyperspectral multiple approach fusion for the long range detection of low observable objects: MUF2. Proc. SPIE, 2006, **6396**, 63960C.1–63960C.12.
5 Vagni, F. 'Survey of hyperspectral and multispectral imaging technologies', RTO Technical Report TR-SET-065-P3, NATO AC/323(SET-065)TP/44, NATO RTO, Brussels Belgium, 2007.
6 Bannon, D. and Thomas, R. 'Meeting the optical demands of next generation hyperspectral imaging spectrometers', http://www.headwallphotonics.com/downloads/photonics_tech_briefs.pdf
7 Aikio, M. 'Hyperspectral prism grating prism imaging spectrograph', ScD thesis, University of Oulu, Oulu, Finland, 2001.
8 Gat, N. Imaging spectroscopy using tunable filters: a review. Proc. SPIE, 2000, **4056**, 50–64.
9 Rajwa, B., Ahmed, W., Venkatapathi, M., Gregori, G., Jin, F., Soos, J., Trivedi, S. and Robinson, J. P. AOTF-based system for image cytometry. Proc. SPIE, 2005, **5694**, 16–23.
10 Fong, A. and Wachman, E. Hyperspectral Imaging for the Life Sciences and Beyond, 2008 (Laurin Publishing, Pittsfield, MA).
11 Pannell, C., Wachman, E., Farkas, D., Ward, J. and Seale, W. Acousto-optic tuneable filters: advances and applications to microscopy. Proc. SPIE, **6088**, 263–272.
12 Manolakis, D. and Shaw, G. Detection algorithms for hyperspectral imaging applications. IEEE Signal Process. Mag., 2002, **19**, 29–43.
13 Stein, D., Beaven, S., Hoff, L., Winter, E., Schaum, A. and Stocker, A. Anomaly detection from hyperspectral imagery. IEEE Signal Process. Mag., 2002, **19**, 58–69.
14 Yu, X. L., Reed, I. S. and Stocker, A. D. Comparative performance analysis of adaptive multispectral detectors. IEEE Trans. Signal Process., 1993, **41**, 2639–2655.
15 Chang, C. I. and Chiang, S. S. Anomaly detection and classification for hyperspectral imagery. IEEE Trans. Geosci. Remote Sens., 2002, **40**, 1314–1325.
16 Muhammed, H. H. Hyperspectral crop reflectance data for characterising and estimating fungal disease severity in wheat. Biosyst. Eng., 2005, **91**, 9–20.
17 Kwon, H. and Nasrabadi, N. Hyperspectral anomaly detection sing kernel RX-algorithm, Proc. IEEE Int. Conf. on Image Processing: ICIP 2004, Singapore, October 2004, IEEE, pp. 3331–3334.
18 Kwon, H. and Nasrabadi, N. Kernel RX-algorithm: a nonlinear anomaly detector for hyperspectral imagery. IEEE Trans. Geosci. Remote Sens., 2005, **43**, 388–397.
19 Yuen, P. and Bishop, G. Adaptive feature extraction techniques for subpixel target detections in hyperspectral remote sensing. Proc. SPIE, **5613**, 99–110.
20 Yuen, P. People tracking without prior information – a biological cortex-like neural approach. Proc. SPIE, **7119**, 711908–711908-11.
21 Duda, R. O., Hart, P. E. and Stork, D. G. Pattern Classification, 2000, 2nd edition (John Wiley & Sons, New York).
22 Ibrahim, I., Yuen, P., Tsitiridis, A., Chen, T., Hong, K., Jackman, J., James, D. and Richardson, M. A. Illumination independent object recognitions using multispectral imaging technique, Proc. SPIE European Sympos. on Optics/photonics in security & defence, Toulouse, France, September 2010, SPIE. 2
23 Yuen, P. and Bishop, G. Enhancements of target detection using atmospheric correction preprocessing techniques in hyperspectral remote sensing. Proc. SPIE, **5613**, 111–118.
24 Yuen, P., Ibrahim, I., Tsitiridis, A., Chen, T., Hong, K., Jackman, J., James, D. and Richardson, M. A. Classification enhancements in hyperspectral remote sensing using atmospheric correction preprocessing technique. Bul. Tekn. S&T Pertahanan, 2009, 91–99. 3

The Imaging Science Journal imsIR6.3d 13/7/10 09:03:09
The Charlesworth Group, Wakefield +44(0)1924 369598 - Rev 7.51n/W (Jan 20 2003)

25 Yuen, P., Chen, T., Hong, K., Tsitiridis, A., Jackman, J., James, D., Richardson, M. A., Oxford, W., Piper, J., Thomas, F. and Lightman, S. Remote detection of stress using hyperspectral imaging technique, Proc. 3rd Int. Conf. on Imaging for crime detection and prevention: ICDP-09, London, UK, December 2009, Kingston University.

26 Zuzak, K. J., Schaeberle, M. D. and Lewis, E. N. Visible reflectance hyperspectral imaging: characterization of a noninvasive, *in vivo* system for determining tissue perfusion. Anal. Chem., 2002, **74**, 2021–2028.

27 Zuzak, K., Gladwin, M., Cannon, R. and Levin, I. Imaging hemoglobin oxygen saturation in sickle cell disease patients using noninvasive visible reflectance hyperspectral techniques: effects of nitric oxide. Am. J. Physiol. Heart Circ. Physiol., 2003, **285**, H1183–H1189.

The Imaging Science Journal imsIR6.3d 13/7/10 09:03:09
The Charlesworth Group, Wakefield +44(0)1924 369598 - Rev 7.51n/W (Jan 20 2003)

Authors Queries

Journal: **The Imaging Science Journal**
Paper: **IR6**
Title: **An introduction to hyperspectral imaging and its application for security, surveillance and target acquisition**

Dear Author
During the preparation of your manuscript for publication, the questions listed below have arisen. Please attend to these matters and return this form with your proof. Many thanks for your assistance

Query Reference	Query	Remarks
1	Author: Please confirm the running head.	
2	Author: Please update information and supply page no.	
3	Author: Please supply volume no.	
4	Author: Please supply page/ paper no.	